Ceramics International 46 (2020) 6906–6913

Contents lists available at ScienceDirect

Ceramics International

journal homepage: www.elsevier.com/locate/ceramint

Thermal conductivity and hardness of three single-phase high-entropy metal diborides fabricated by borocarbothermal reduction and spark plasma sintering

Joshua Gild[a], Andrew Wright[b], Kathleen Quiambao-Tomko[c], Mingde Qin[a], John A. Tomko[d], Md Shafkat bin Hoque[c], Jeffrey L. Braun[c], Blake Bloomfield[b], Daniel Martinez[b], Tyler Harrington[a], Kenneth Vecchio[a,b], Patrick E. Hopkins[c,d,e], Jian Luo[a,b,*]

[a] *Program of Materials Science and Engineering, University of California, San Diego, La Jolla, CA, 92093-0418, USA*
[b] *Department of NanoEngineering, University of California, San Diego, La Jolla, CA, 92093-0448, USA*
[c] *Department of Mechanical and Aerospace Engineering, University of Virginia, Charlottesville, VA, 22904, USA*
[d] *Department of Materials Science and Engineering, University of Virginia, Charlottesville, VA, 22904, USA*
[e] *Department of Physics, University of Virginia, Charlottesville, VA, 22904, USA*

ARTICLE INFO

Keywords:
High-entropy ceramics
Borocarbothermal reduction
Boride
Thermal conductivity

ABSTRACT

Four high-entropy metal diborides have been synthesized and densified by borocarbothermal reduction of metal oxides with boron carbide and graphite and subsequent spark plasma sintering. Three of them, $(Hf_{0.2}Zr_{0.2}Ti_{0.2}Ta_{0.2}Nb_{0.2})B_2$, $(Hf_{0.2}Zr_{0.2}Ti_{0.2}Ta_{0.2}Mo_{0.2})B_2$, and $(Hf_{0.2}Zr_{0.2}Ti_{0.2}Ta_{0.2}Cr_{0.2})B_2$, possess single high-entropy phases and have been sintered to > 99% of the theoretical densities. The fourth $(Hf_{0.2}Zr_{0.2}Ti_{0.2}Mo_{0.2}W_{0.2})B_2$ specimen contained a Ti–Mo–W rich secondary phase in addition to the primary metal diboride phase. The specimens made by borocarbothermal reduction exhibit improved hardnesses in comparison with those samples previously fabricated via high energy ball milling and spark plasma sintering. Interestingly, the single-phase $(Hf_{0.2}Zr_{0.2}Ti_{0.2}Ta_{0.2}Mo_{0.2})B_2$ and $(Hf_{0.2}Zr_{0.2}Ti_{0.2}Ta_{0.2}Cr_{0.2})B_2$ (both of which have Vickers hardness values of ~25 GPa) are substantially harder than $(Hf_{0.2}Zr_{0.2}Ti_{0.2}Ta_{0.2}Nb_{0.2})B_2$ (20.5 GPa), despite MoB_2 and CrB_2 being typically considered as softer components. These single-phase high-entropy metal diborides were found to have low thermal conductivities of 12–25 W/mK, which are ~1/10 to ~1/5 of the reported values of HfB_2 and ZrB_2.

1. Introduction

High-entropy alloys typically refer to metallic alloys with five or more elements of equimolar or near equimolar concentrations and a molar configurational entropy of $> \sim 1.6R$, where R is the gas constant [1–3]. Since 2015, the field has expanded to include various high-entropy ceramics that have been fabricated in the bulk form, including high-entropy metal diborides [4,5], carbides [6–8], nitrides [9,10], sulfides [11], silicides [12,13], as well as fluorite [14,15], spinel [16,17], rocksalt [18], magnetoplumbite [19], and silicate oxides [20]. Among these high-entropy materials, a few of them have been proven to be true entropy-stabilized materials [6,18]. In particular, high-entropy metal diborides, a new class of ultrahigh temperature ceramics (UHTCs) first reported in 2016 [9], proved to be difficult to sinter to high densities with minimum native oxide contamination. In the initial work, six single-phase, high-entropy metal diborides were synthesized via high energy ball milling of commercial powders and spark plasma sintering [9]. While this procedure allowed for the rapid testing of multiple high-entropy compositions, it left undesirable oxide inclusions and resulted in low relative densities of ~91–93%. The difficulty in producing fully dense metal diboride specimens can be attributed to two reasons: (1) the strong chemical bonds that leads to slow diffusion and (2) oxygen contamination that promote coarsening at the expense of densification.

To mitigate these issues, fine powders with little oxygen contamination and/or novel sintering routes are needed. To pursue this, Tallartia et al. achieved similar densities without the oxide inclusions via self-propagating synthesis of metal and boron powder [21]. Gild et al. achieved > 99% density via reactive flash spark plasma sintering with addition of carbon [22]. Moreover, a substantial body of work on the direct synthesis of individual diboride powders, especially ZrB_2

---

[*] Corresponding author. Program of Materials Science and Engineering, University of California, San Diego, La Jolla, CA, 92093-0418, USA.
E-mail address: jluo@alum.mit.edu (J. Luo).

https://doi.org/10.1016/j.ceramint.2019.11.186
Received 7 October 2019; Received in revised form 14 November 2019; Accepted 20 November 2019

Table 1

Summary of the measured lattice parameters, grain size, and Vickers hardness of four specimens. Excess B_4C amounts needed in the borocarbothermal reduction synthesis for making single-phase samples are also listed for each case. Noting that these are not the remaining B_4C phase in the final sintered specimens, which are < 1 vol% in all cases.

Compositions	Excess B_4C Needed/ Added in Synthesis [wt %]	Lattice Parameters		Measured/Theoretical Density [g/cm^3] (Relative Density)	Vickers Hardness [GPa]	Grain Size [μm]	Thermal Conductivity [W/mK]
		a [Å]	c [Å]				
$(Hf_{0.2}Zr_{0.2}Ti_{0.2}Ta_{0.2}Nb_{0.2})B_2$	15	3.097	3.372	8.25/8.29 (99.5%)	20.5 ± 1.0	3.4 ± 1.3	24.8 ± 5.1
$(Hf_{0.2}Zr_{0.2}Ti_{0.2}Ta_{0.2}Mo_{0.2})B_2$	14	3.092	3.366	8.35/8.37 (99.9%)	24.9 ± 1.0	6.8 ± 4.0	15.2 ± 3.5
$(Hf_{0.2}Zr_{0.2}Ti_{0.2}Ta_{0.2}Cr_{0.2})B_2$	5	3.086	3.356	7.83/7.90 (99.1%)	24.9 ± 1.0	4.5 ± 1.9	12.6 ± 2.5
$(Hf_{0.2}Zr_{0.2}Ti_{0.2}Mo_{0.2}W_{0.2})B_2$	15	3.084	3.357	–	29.4 ± 1.7	4.3 ± 1.8	–

[23–27], motivated several groups to apply similar methods to fabricate high-entropy metal diborides. In this regard, Zhang et al. fabricated high-entropy powder via borothermal synthesis but significant oxide inclusions still remained in the final sintered specimen [28]. Similarly, Shen et al. fabricated $(Hf_{0.2}Zr_{0.2}Ti_{0.2}Ta_{0.2}Nb_{0.2})B_2$ powder and densified it with silicon carbide via spark plasma sintering (SPS) [29]. Moreover, Liu et al. fabricated $(Hf_{0.2}Zr_{0.2}Ti_{0.2}Ta_{0.2}Nb_{0.2})B_2$ and $(Hf_{0.2}Ti_{0.2}Ta_{0.2}Nb_{0.2})B_2$ powders via borothermal and borocarbothermal reductions utilizing boron and boron carbide plus carbon, respectively, as reducing agents. While they produced fine, single-phase powders, they did not investigate their sinterability or subsequent properties [30,31]. During the preparation of the current manuscript, we noticed that Gu et al. reported the successful fabrication of fully-dense and oxide-free $(Hf_{0.2}Zr_{0.2}Ti_{0.2}Ta_{0.2}Nb_{0.2})B_2$ via a similar borocarbothermal synthesis route [26] concurrently with our study.

In this work, we examined a borocarbothermal reduction synthesis plus SPS route to successfully fabricate fully-dense (> 99%), oxide-free, high-entropy metal diborides of four compositions: $(Hf_{0.2}Zr_{0.2}Ti_{0.2}Ta_{0.2}Nb_{0.2})B_2$, $(Hf_{0.2}Zr_{0.2}Ti_{0.2}Ta_{0.2}Mo_{0.2})B_2$, $(Hf_{0.2}Zr_{0.2}Ti_{0.2}Ta_{0.2}Cr_{0.2})B_2$, and $(Hf_{0.2}Zr_{0.2}Ti_{0.2}Mo_{0.2}W_{0.2})B_2$. The first three of them were successfully made into single-phase.

In addition to the borocarbothermal reduction synthesis method, our study also revealed two new findings. First, we made a surprising observation of enhanced hardness for high-entropy compositions containing Mo and Cr, which are typically considered to be softening components [32]. Second, we report (and confirm) the substantially reduced thermal conductivities of the single-phase high-entropy metal diborides, for the first time to our knowledge, albeit similar trends are known for other high-entropy ceramics [12,14,33–35].

2. Materials and methods

2.1. Borocarbothermal reduction synthesis

The raw materials for borocarbothermal synthesis were powders of HfO_2, ZrO_2, Nb_2O_5, Ta_2O_5, TiO_2, MoO_3, WO_3, Cr_2O_3 (≥99% purity; ≥45 μm purchased from Alfa Aesar, MA, USA), B_4C, C (≥99.9% purity; 1–3 μm, 0.4–1.2 μm, respectively, purchased from US Research Nanomaterials, TX, USA). Appropriate amounts of five individual metal diboride powders were weighed according to the targeted stoichiometries (calculated on a metals basis): $(Hf_{0.2}Zr_{0.2}Ti_{0.2}Ta_{0.2}Nb_{0.2})B_2$, $(Hf_{0.2}Zr_{0.2}Ti_{0.2}Ta_{0.2}Mo_{0.2})B_2$, $(Hf_{0.2}Zr_{0.2}Ti_{0.2}Ta_{0.2}Cr_{0.2})B_2$, and $(Hf_{0.2}Zr_{0.2}Ti_{0.2}Mo_{0.2}W_{0.2})B_2$. The nominal chemical reactions are:

$$2HfO_2 + 2ZrO_2 + 2TiO_2 + Ta_2O_5 + Nb_2O_5 + 3C + 7B_4C \rightarrow 2(Hf_{0.2}Zr_{0.2}Ti_{0.2}Ta_{0.2}Nb_{0.2})B_2 + 4B_2O_3 + 10CO \quad (1)$$

$$12HfO_2 + 12ZrO_2 + 12TiO_2 + 6Ta_2O_5 + 12MoO_3 + 31C + 41B_4C \rightarrow 12(Hf_{0.2}Zr_{0.2}Ti_{0.2}Ta_{0.2}Mo_{0.2})B_2 + 22B_2O_3 + 72CO \quad (2)$$

$$24HfO_2 + 24ZrO_2 + 24TiO_2 + 12Ta_2O_5 + 12Cr_2O_3 + 33C + 81B_4C \rightarrow 24(Hf_{0.2}Zr_{0.2}Ti_{0.2}Ta_{0.2}Cr_{0.2})B_2 + 42B_2O_3 + 114CO \quad (3)$$

$$7HfO_2 + 7ZrO_2 + 7TiO_2 + 7MoO_3 + 7WO_3 + 27B_4C \rightarrow 7(Hf_{0.2}Zr_{0.2}Ti_{0.2}Mo_{0.2}W_{0.2})B_2 + 19B_2O_3 + 27CO \quad (4)$$

Due to the possible residual oxide present in boron carbide, the possible carbon deficiencies in boron carbide (nominally B_4C) [36], and the possible formation of volatile boron suboxide such as B_2O_2 (instead of B_2O_3) [37], the addition of an excess amount of boron carbide or carbon is typically necessary [24,27,36,38–40]. We acknowledge that Liu et al. have investigated the possible origins of oxygen impurities in high-entropy metal diboride made by via borocarbothermal reduction, including possible other reactions that consume the excess amounts of B_4C [30]. We have optimized the excess amounts of B_4C used for each composition to ensure the formation of dense metal diborides with both minimum oxide and minimum remaining B_4C (< 1 vol%) in the final sintered specimens; these optimal amounts are given in Table 1 for each of the four cases. We note that in Eq. (4) that carbon was not used as a precursor in the tungsten containing sample due to the high stability of WC relative to the diboride structure. The amount of excess B_4C needed, 5–15 wt%, is similar to the amount needed for the borocarbothermal synthesis of HfB_2 [24] and ZrB_2 [38,41], which were attributed to the loss of boron oxide due to high vapor pressure under vacuum at elevated temperatures. The addition of excess carbon in these studies increased the probability of forming a carbide phase; therefore, carbon was not added in the current study.

For borocarbothermal synthesis, the mixture of five metal oxide powders were initially milled for 48 h in zirconia jars at 200 rpm in acetone with YSZ media. Subsequently, the milled oxides, boron carbide, and graphite were planetary milled for 2 h at 200 rpm in acetone in polytetrafluoroethylene (PTFE) jars with YSZ media. The powder was then dried in a rotary evaporator after both milling steps. The powder mixture was lightly pressed into 25 mm pellets to ensure good contact of the particles in the powder. The pellets were loaded into a graphite furnace (Red Devil, RDWebb, Natick, MA, USA) that was pumped down to 1×10^{-1} bar and backfilled with argon twice before a turbomolecular pump was engaged to pump the chamber down to 1×10^{-4} bar. The furnace, while under vacuum, was heated to 1475 °C at a rate of 10 °C/min, held at 1475 °C for 15 min to allow for calibration of the pyrometer, and heated to 1550 °C at a rate of 5 °C/min. It was held at 1550 °C for 90 min to allow for the evaporation of boron oxide and then cooled naturally. Upon removal from the furnace, the powder was immediately quenched in liquid nitrogen to prevent oxygen contamination and moved into an argon glovebox. All dies with this powder were assembled in a glovebox to prevent oxidation.

The powders were densified into 20-mm diameter disks via spark plasma sintering (SPS, Thermal Technologies, CA, USA) at 2000 °C for 30 min under an initial uniaxial pressure of 80 MPa, which was lowered to 30 MPa after 5 min at 2000 °C to prevent creep of the graphite tooling, with a heating ramping rate of 100 °C/min. The chamber was initially pumped down to vacuum of at least 2×10^{-2} Torr prior to the SPS experiments and backfilled with argon gas twice to minimize oxygen contamination from the chamber. The run was performed under vacuum until 2000 °C when argon was introduced. The graphite die was lined with 125 μm thick graphite paper to prevent reaction of the specimen with the die. Upon completion, the samples cooled naturally in the SPS machine.

2.2. Characterization

Densities were calculated via the Archimedes method. The relative densities were calculated utilizing theoretical densities computed based on an ideal stoichiometry and the lattice parameter measured by X-ray diffraction (XRD).

All sintered specimens were characterized by X-ray diffraction (XRD) utilizing a Rigaku diffractometer with Cu Kα radiation. Field emission scanning electron microscopy (FE SEM) images, electron dispersive X-ray spectroscopy (EDS), and electron backscatter diffraction (EBSD) data were collected from specimens utilizing a FEI Apreo microscope equipped with an Oxford N-Max^{N} EDS detector and Oxford Symmetry EBSD detector.

Vickers hardness measurements were performed on specimens of all four compositions. Hardness measurements were performed with a Vickers' diamond indenter at 200 gf/mm^2 with a hold time of 15 s. The indentations were examined for conformation with the standard ASTM C1327. The indentations averaged 20–25 μm in width during the testing. Twenty-five measurements were performed at different locations of each specimen; the mean and standard deviation are reported.

Thermal conductivities were measured using time-domain thermoreflectance (TDTR) [42–44] on three single-phase samples with composition $(Hf_{0.2}Zr_{0.2}Ti_{0.2}Ta_{0.2}X_{0.2})B_2$, where X is Nb, Mo, or Cr. The HEB specimens subjected to TDTR testing were selected in order to elucidate the change in thermal conductivity while varying a single element in the composition. A thin Al transducer (84 ± 4 nm) is electron beam deposited onto the sample, which acts as an optical transducer. Using a Ti:Sapphire laser emitting a train of < 200 fs pulses at a central wavelength of 800 nm and a repetition rate of 80 MHz, the output is divided into a pump and probe path. The pump is modulated at 8.4 MHz to heat the sample, while the probe is used to measure the resulting change in temperature as a function of delay time out to 5.5 ns after pump absorption. The pump and probe $1/e^2$ diameters are 24 and 11 μm, respectively. The volumetric heat capacity was taken to be 2.5 ± 0.3 J cm^{-3} K^{-1} based on the rule of mixtures average of constituent heat capacities [45].

3. Results and discussion

3.1. Borocarbothermal reduction synthesis powders

The XRD of a diboride powder after the borocarbothermal reduction

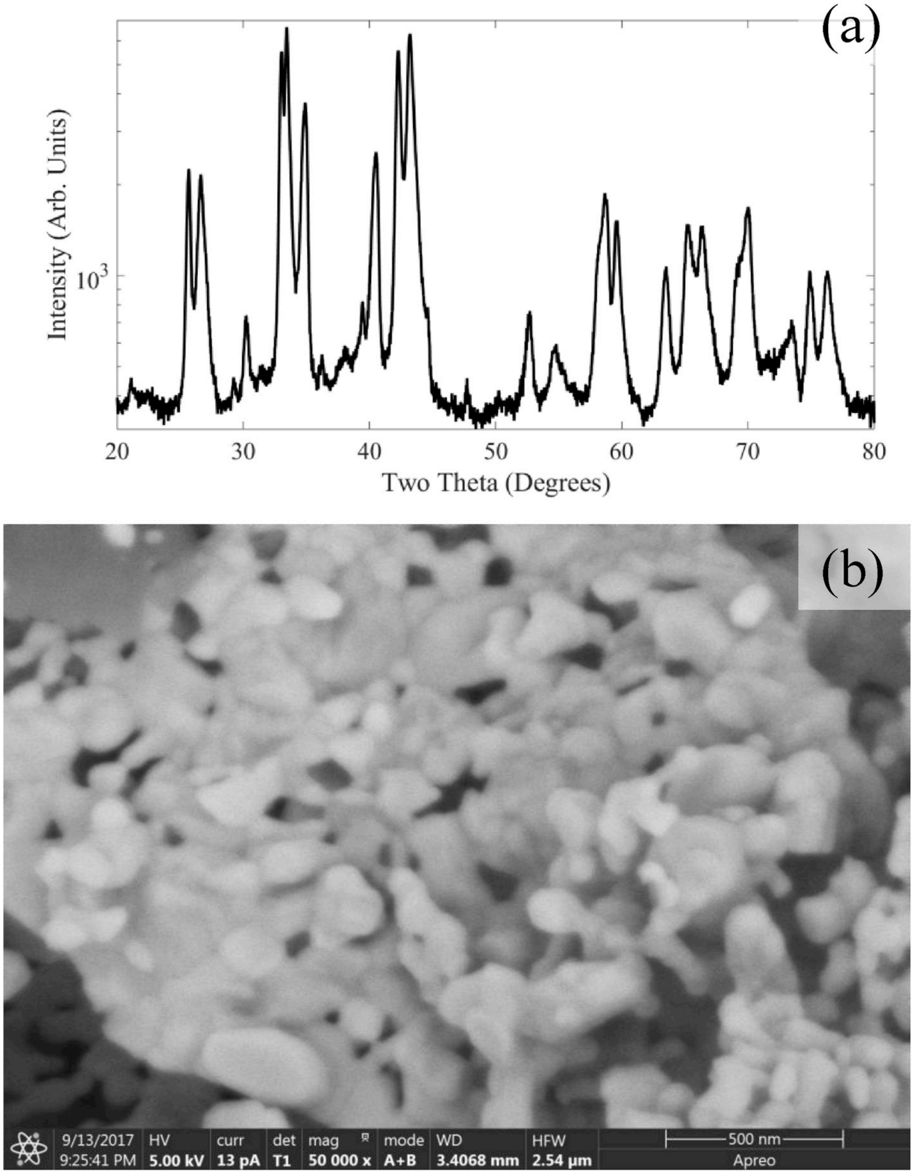

Fig. 1. (a) XRD pattern of as-synthesized powder, showing multiple phases after the borocarbothermal reduction. Noting that the XRD intensity is plotted in a logarithmical scale. (b) SEM image of the as-synthesized powder.

synthesis shows the presence of multiple diboride phases with broad peaks (Fig. 1a). This is to be expected as the temperatures of the synthesis were not sufficiently high to allow for the formation of a single high-entropy diboride phase. The lattice parameters of the individual diborides are similar so that multiple phases can manifest as peak broadening for polydisperse particle size powder. No refractory metal oxide peaks nor boron carbide peaks were observed in XRD. SEM characterization of the powder showed the particle sizes to be between 200 and 500 nm, as shown in Fig. 1b.

3.2. Phase formation and compositional uniformity

On the one hand, XRD patterns of sintered $(Hf_{0.2}Zr_{0.2}Ti_{0.2}Ta_{0.2}Nb_{0.2})B_2$, $(Hf_{0.2}Zr_{0.2}Ti_{0.2}Ta_{0.2}Mo_{0.2})B_2$, and $(Hf_{0.2}Zr_{0.2}Ti_{0.2}Ta_{0.2}Cr_{0.2})B_2$ (after SPS) showed single, hexagonal, metal diboride phase (Fig. 2). The lattice parameters of the specimens are given in Table 1. EDS confirms elemental uniformity of these three compositions (Fig. 3), which are notably more homogenous than the first high-entropy fabrication work utilizing high-energy ball milling [4] as well as the recent borothermal reduction synthesis work by Zhang et al. [28]. Moreover, we did not observe any residual hafnium or zirconium oxide secondary phases which were prevalent in Zhang et al. recent borothermal reduction synthesis work [28]. Similar results were observed by Tallarita et al. with powder produced via self-heating synthesis and subsequent densification via spark plasma sintering, although they only achieved 92.5% relative density [21]. The $(Hf_{0.2}Zr_{0.2}Ti_{0.2}Ta_{0.2}Nb_{0.2})B_2$ and its composites with SiC made by Shen et al. also contained residual hafnium and zirconium oxide, though their samples were otherwise chemically homogenous [29]. In the work conducted concurrently by Gu et al. [26], borocarbothermal reduction synthesized $(Hf_{0.2}Zr_{0.2}Ti_{0.2}Ta_{0.2}Nb_{0.2})B_2$ showed comparable phase formation, chemical homogeneity, density, and lattice parameters to ours for $(Hf_{0.2}Zr_{0.2}Ti_{0.2}Ta_{0.2}Nb_{0.2})B_2$ (albeit they only reported one composition).

On the other hand, $(Hf_{0.2}Zr_{0.2}Ti_{0.2}Mo_{0.2}W_{0.2})B_2$ formed a mixture of a primary high-entropy diboride phase and a secondary molybdenum and tungsten rich phase.

The composition was mesaured by EDS point analysis (Fig. 4). This secondary phase is mostly rich in Mo and W, with a significant amount of Ti.

3.3. Density

Samples sintered from borocarbothermal reduction synthesized powders possessed high relative density; e.g., the $(Hf_{0.2}Zr_{0.2}Ti_{0.2}Ta_{0.2}Nb_{0.2})B_2$ achieved a relative density of 99.4%, versus 93% in the first fabricated high-entropy boride of the identical composition made by high-energy ball milling and SPS [4]. Similar high relative densities have been achieved for $(Hf_{0.2}Zr_{0.2}Ti_{0.2}Ta_{0.2}Mo_{0.2})B_2$, 99.7%, and $(Hf_{0.2}Zr_{0.2}Ti_{0.2}Ta_{0.2}Cr_{0.2})B_2$, 99.1%.

Due to the presence of a secondary phase in $(Hf_{0.2}Zr_{0.2}Ti_{0.2}Mo_{0.2}W_{0.2})B_2$, the theoretical density, and therefore the relative density, could not be accurately determined. From image analysis, the relative density also appears to be greater than 99% (i.e., with less than 1 vol% of pores and residual B_4C/C phase in total).

3.4. Vickers hardness

The measured Vickers hardness values of the metal diborides specimens are given in Table 1. $(Hf_{0.2}Zr_{0.2}Ti_{0.2}Ta_{0.2}Nb_{0.2})B_2$ possesses a hardness of 20.5 ± 1.0 GPa. Notably, Vickers hardness values of both $(Hf_{0.2}Zr_{0.2}Ti_{0.2}Ta_{0.2}Mo_{0.2})B_2$ and $(Hf_{0.2}Zr_{0.2}Ti_{0.2}Ta_{0.2}Cr_{0.2})B_2$ were measured to be ~24.9 ± 1.0 GPa. These values are in the same range of those of dense individual metal diborides reported in literature: ZrB_2 (23.0 GPa) [48], HfB_2 (28 GPa) [49], TaB_2 (25.6 GPa) [50], and TiB_2 (19–26 GPa) [51], but substantially higher to that of CrB_2 (15.9 GPa) [52], albeit vastly different fabrication methods and microstructures. For more direct comparisons within high-entropy metal diborides, the measured Vickers hardness of these specimens are notably higher than those of the first fabricated high-entropy metal diborides via mechanical alloying and spark plasma sintering (17.5–19.9 GPa) [4] but are comparable with the most recent report of a $(Hf_{0.2}Zr_{0.2}Ti_{0.2}Ta_{0.2}Nb_{0.2})B_2$ fabricated by a similar borocarbothermal reduction route (22.5 GPa) [26].

In particular, it is interesting to note that both $(Hf_{0.2}Zr_{0.2}Ti_{0.2}Ta_{0.2}Mo_{0.2})B_2$ and $(Hf_{0.2}Zr_{0.2}Ti_{0.2}Ta_{0.2}Cr_{0.2})B_2$ (containing 20 mol% MoB_2 and CrB_2, respectively) are substantially (~4.4 GPa) harder than $(Hf_{0.2}Zr_{0.2}Ti_{0.2}Ta_{0.2}Nb_{0.2})B_2$ (all made by the same route with > 99% density and are oxide free) because MoB_2 and CrB_2 are expected to possess substantially lower hardness than all the Group IV diborides [32]. At least one experiment measured the Vickers hardness of a CrB_2 specimen to be 15.9 GPa [52]. Noting that MoB_2 is not a stable phase at room temperature (so that there is no experimental data of hardness), but lower hardness was predicted by DFT calculations [32].

The two-phase $(Hf_{0.2}Zr_{0.2}Ti_{0.2}Mo_{0.2}W_{0.2})B_2$ showed a higher hardness of 29.4 ± 1.7 GPa. The observed increased hardness is not surprising for a composition containing a tungsten rich boride phase, as some boride phases can be harder, e.g., tungsten tetraboride is an ultrahard ceramic [46,47]. The presence of a (perhaps harder) secondary phase can increase the hardness of this two-phase composite via composite and/or microstructural effects.

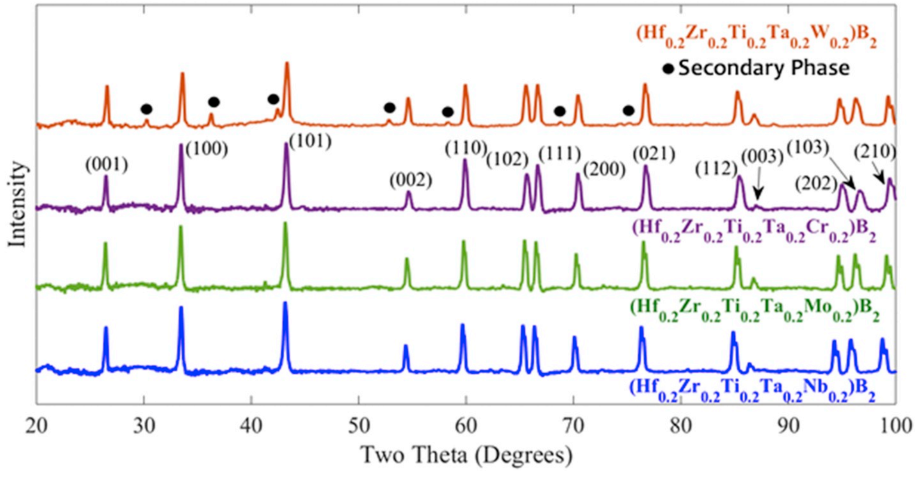

Fig. 2. XRD patterns (with the intensities plotted in logarithmical scales) of the four high-entropy diboride specimens after SPS. Three of them, $(Hf_{0.2}Zr_{0.2}Ti_{0.2}Ta_{0.2}Nb_{0.2})B_2$, $(Hf_{0.2}Zr_{0.2}Ti_{0.2}Ta_{0.2}Mo_{0.2})B_2$, and $(Hf_{0.2}Zr_{0.2}Ti_{0.2}Ta_{0.2}Cr_{0.2})B_2$, exhibit single high entropy phases. The fourth specimen, $(Hf_{0.2}Zr_{0.2}Ti_{0.2}Mo_{0.2}W_{0.2})B_2$, has a minor amount of a secondary phase.

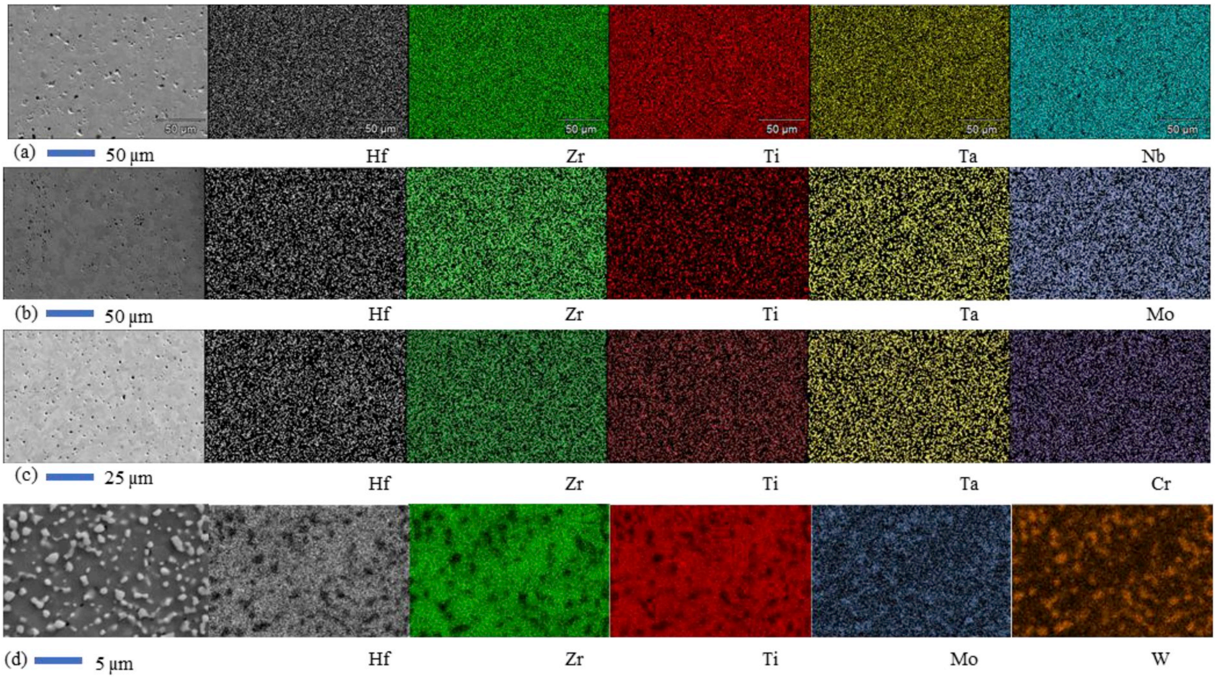

Fig. 3. Cross-sectional SEM images and the corresponding EDS elemental maps of the sintered (a) $(Hf_{0.2}Zr_{0.2}Ti_{0.2}Ta_{0.2}Nb_{0.2})B_2$, (b) $(Hf_{0.2}Zr_{0.2}Ti_{0.2}Ta_{0.2}Mo_{0.2})B_2$, (c) $(Hf_{0.2}Zr_{0.2}Ti_{0.2}Ta_{0.2}Cr_{0.2})B_2$, and (d) $(Hf_{0.2}Zr_{0.2}Ti_{0.2}Mo_{0.2}W_{0.2})B_2$ specimens.

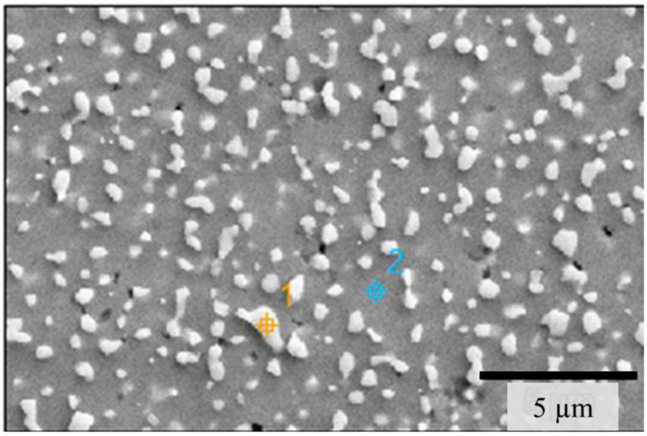

	Hf	Zr	Ti	Mo	W	Ir
Point 1	4.9	0.0	10.0	22.3	60.7	2.2
Point 2	25.4	17.9	25.1	7.6	20.2	3.9

Fig. 4. Point EDS analysis of the sintered $(Hf_{0.2}Zr_{0.2}Ti_{0.2}Mo_{0.2}W_{0.2})B_2$ specimen, showing a tungsten and molybdenum rich secondary phase. The iridium detected was from the sputtered conductive coating in SEM specimen preparation.

3.5. *Electron backscatter diffraction*

EBSD was utilized to measure the grain size and examine the texture of the sintered specimens. EBSD maps and their distributions are shown in Fig. 5. No significant texturing was evident in any samples.

The measured average grain sizes (± one standard deviations) are 3.4 ± 1.3 μm for $(Hf_{0.2}Zr_{0.2}Ti_{0.2}Ta_{0.2}Nb_{0.2})B_2$, 6.8 ± 4.0 μm for $(Hf_{0.2}Zr_{0.2}Ti_{0.2}Ta_{0.2}Mo_{0.2})B_2$, and 4.5 ± 1.9 μm for $(Hf_{0.2}Zr_{0.2}Ti_{0.2}Ta_{0.2}Cr_{0.2})B_2$, respectively, for three single-phase specimens. Specifically, the grain size of $(Hf_{0.2}Zr_{0.2}Ti_{0.2}Ta_{0.2}Nb_{0.2})B_2$ is also similar to that observed by Gu et al. for the same composition after SPS at 2000 °C [26].

The measured average grain size is 4.3 ± 1.8 μm for the (primary) high-entropy metal diboride phase in the two-phase $(Hf_{0.2}Zr_{0.2}Ti_{0.2}Mo_{0.2}W_{0.2})B_2$. The secondary phase was measured to be approximately 10 vol% of the sample by EBSD.

3.6. *Thermal conductivity*

The measured thermal conductivities are listed in Table 1. The thermal conductivities were measured to be 24.8 ± 5.1 W m^{-1} K^{-1} for $(Hf_{0.2}Zr_{0.2}Ti_{0.2}Ta_{0.2}Nb_{0.2})B_2$, 15.2 ± 3.5 W m^{-1} K^{-1} for $(Hf_{0.2}Zr_{0.2}Ti_{0.2}Ta_{0.2}Mo_{0.2})B_2$, 12.6 ± 2.5 W m^{-1} K^{-1} for $(Hf_{0.2}Zr_{0.2}Ti_{0.2}Ta_{0.2}Cr_{0.2})B_2$ for the three single-phase samples. The uncertainties in these measured values of thermal conductivity arise from a combination of sources, including the uncertainty in our Al transducer thickness, uncertainty in our assumed heat capacity (discussed in Section 2.2), and the standard deviation about the mean value determined from multiple TDTR measurements on different locations on the sample.

These values are significantly lower than those observed in monolithic diborides. Specifically, HfB_2 and ZrB_2 have reported thermal conductivities values of over 100 W m^{-1} K^{-1}, though the actual numbers can heavily depend on the processing conditions and microstructure (where the values are lower in cases with porosity and impurities) [49,53,54]. TiB_2 possesses a thermal conductivity up to 96 W m^{-1} K^{-1} [51,55]. CrB_2 has a conductivity of 22.3 W m^{-1} K^{-1}, though the density and microstructure of the specimen is not mentioned in the paper [56]. Thus, the thermal conductivities of the high-entropy systems are substantially lower than most monolithic metal diborides and only ~1/5 to ~1/10 of that of HfB_2 or ZrB_2, depending on the specific composition. This is similar to the observed reduction in thermal conductivities in $(Mo_{0.2}Nb_{0.2}Ta_{0.2}Ti_{0.2}W_{0.2})Si_2$ [12], high-entropy rocksalt oxides [33,34], and high-entropy carbides, e.g., $(Hf_{0.2}Zr_{0.2}Ti_{0.2}Ta_{0.2}Nb_{0.2})C$ and $(Zr_{0.2}Nb_{0.2}Ti_{0.2}V_{0.2})C$ [35,57].

While reduced thermal conductivity is expected for high-entropy ceramics due to the increased phonon scattering, it is first confirmed

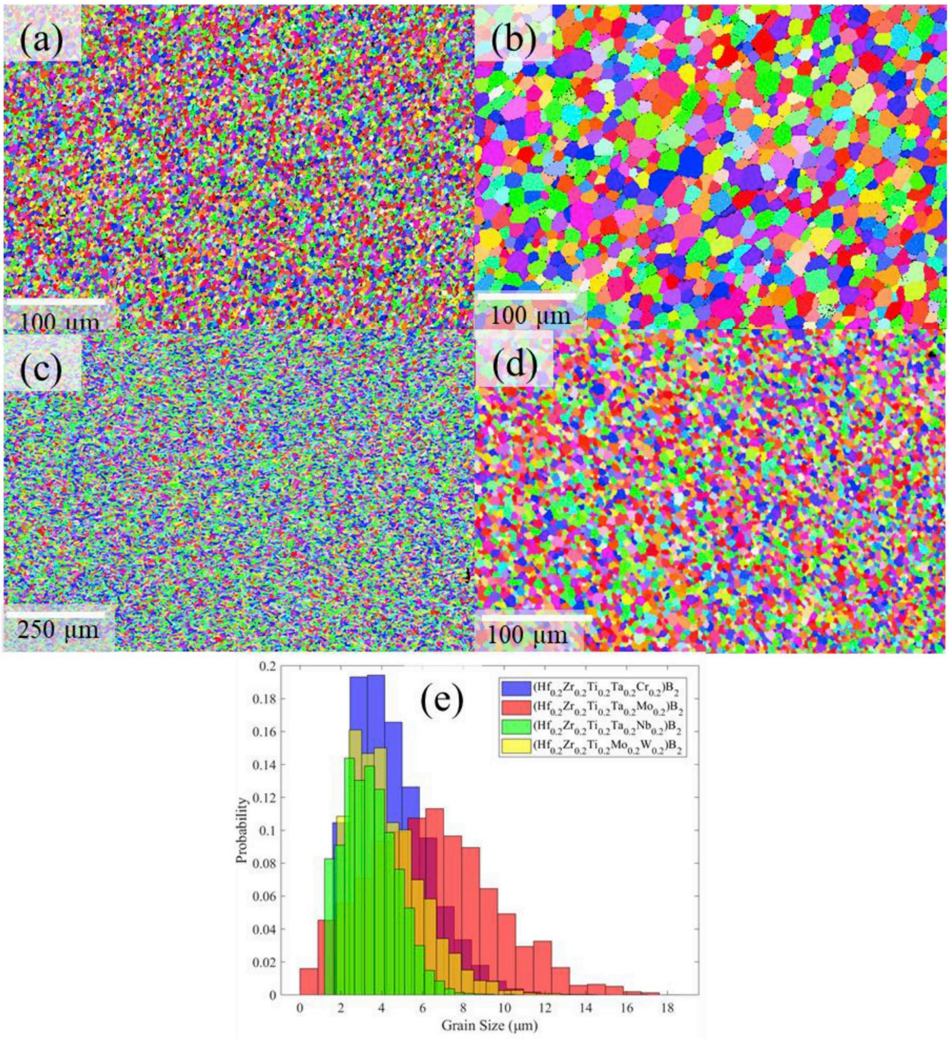

Fig. 5. EBSD maps of (a) $(Hf_{0.2}Zr_{0.2}Ti_{0.2}Ta_{0.2}Nb_{0.2})B_2$, (b) $(Hf_{0.2}Zr_{0.2}Ti_{0.2}Ta_{0.2}Mo_{0.2})B_2$, (c) $(Hf_{0.2}Zr_{0.2}Ti_{0.2}Ta_{0.2}Cr_{0.2})B_2$, and (c) $(Hf_{0.2}Zr_{0.2}Ti_{0.2}Mo_{0.2}W_{0.2})B_2$, along with (e) the grain size distributions.

experimentally for high-entropy metal diborides in this study.

We further note that $(Hf_{0.2}Zr_{0.2}Ti_{0.2}Ta_{0.2}Nb_{0.2})B_2$ has the highest thermal conductivity of these three compositions, which agrees with the DFT predictions by Wang et al. [58].

4. Conclusions

Four high-entropy metal diborides, $(Hf_{0.2}Zr_{0.2}Ti_{0.2}Ta_{0.2}Nb_{0.2})B_2$, $(Hf_{0.2}Zr_{0.2}Ti_{0.2}Ta_{0.2}Mo_{0.2})B_2$, $(Hf_{0.2}Zr_{0.2}Ti_{0.2}Ta_{0.2}Cr_{0.2})B_2$, and $(Hf_{0.2}Zr_{0.2}Ti_{0.2}Mo_{0.2}W_{0.2})B_2$ have been synthesized via borocarbothermal reduction of metal oxide powders and densified via subsequent spark plasma sintering. The samples show high density (> 99%) and hardness, and they are essentially free of observable oxide inclusions. Three of them exhibit single high-entropy phases.

The three single-phase high-entropy metal diborides are measured to have significantly lower thermal conductivity compared to monolithic metal diborides. While reduced thermal conductivity is well expected for high-entropy ceramics, it is confirmed experimentally for high-entropy metal diborides for the first time in this study.

Another scientifically interesting observation is that the single-phase $(Hf_{0.2}Zr_{0.2}Ti_{0.2}Ta_{0.2}Mo_{0.2})B_2$ and $(Hf_{0.2}Zr_{0.2}Ti_{0.2}Ta_{0.2}Cr_{0.2})B_2$ (both of which have Vickers hardness values of ~25 GPa) are harder than $(Hf_{0.2}Zr_{0.2}Ti_{0.2}Ta_{0.2}Nb_{0.2})B_2$ (20.5 GPa), despite MoB_2 and CrB_2 are considered as softer components.

Declaration of competing interest

No conflict of interest.

Acknowledgements

This work is supported by an Office of Naval Research MURI program (Grant No. N00014-15-1-2863; Program Managers: Dr. Kenny Lipkowitz and Dr. Eric Wuchina). We thank all MURI colleagues for helpful scientific discussion. P.E.H. also acknowledges partial support from the National Science Foundation, Grant No. CBET-1706388.

Appendix A. Supplementary data

Supplementary data to this article can be found online at https://doi.org/10.1016/j.ceramint.2019.11.186.

References

[1] D.B. Miracle, O.N. Senkov, A critical review of high entropy alloys and related concepts, Acta Mater. 122 (2017) 448–511, https://doi.org/10.1016/j.actamat.2016.08.081.

[2] J.-W. Yeh, S.-K. Chen, S.-J. Lin, J.-Y. Gan, T.-S. Chin, T.-T. Shun, C.-H. Tsau, S.-Y. Chang, Nanostructured high-entropy alloys with multiple principal elements: novel alloy design concepts and outcomes, Adv. Eng. Mater. 6 (2004) 299–303, https://doi.org/10.1002/adem.200300567.

[3] J.-W. Yeh, S.-J. Lin, T.-S. Chin, J.-Y. Gan, S.-K. Chen, T.-T. Shun, C.-H. Tsau, S.-Y. Chou, Formation of simple crystal structures in Cu-Co-Ni-Cr-Al-Fe-Ti-V alloys with multiprincipal metallic elements, Metall. Mater. Trans. A 35 (2004) 2533–2536, https://doi.org/10.1007/s11661-006-0234-4.

[4] J. Gild, Y. Zhang, T. Harrington, S. Jiang, T. Hu, M.C. Quinn, W.M. Mellor, N. Zhou, K. Vecchio, J. Luo, High-entropy metal diborides: a new class of high-entropy materials and a new type of ultrahigh temperature ceramics, Sci. Rep. 6 (2016) 37946, https://doi.org/10.1038/srep37946.

[5] P.H. Mayrhofer, A. Kirnbauer, Ph Ertelthaler, C.M. Koller, High-entropy ceramic thin films; A case study on transition metal diborides, Scr. Mater. 149 (2018) 93–97, https://doi.org/10.1016/j.scriptamat.2018.02.008.

[6] T.J. Harrington, J. Gild, P. Sarker, C. Toher, C.M. Rost, O.F. Dippo, C. McElfresh, K. Kaufmann, E. Marin, L. Borowski, P.E. Hopkins, J. Luo, S. Curtarolo, D.W. Brenner, K.S. Vecchio, Phase stability and mechanical properties of novel high entropy transition metal carbides, Acta Mater. 166 (2019) 271–280, https://doi.org/10.1016/j.actamat.2018.12.054.

[7] E. Castle, T. Csanádi, S. Grasso, J. Dusza, M. Reece, Processing and properties of high-entropy ultra-high temperature carbides, Sci. Rep. 8 (2018) 8609, https://doi.org/10.1038/s41598-018-26827-1.

[8] L. Feng, W.G. Fahrenholtz, G.E. Hilmas, Y. Zhou, Synthesis of single-phase high-entropy carbide powders, Scr. Mater. 162 (2019) 90–93, https://doi.org/10.1016/j.scriptamat.2018.10.049.

[9] T. Jin, X. Sang, R.R. Unocic, R.T. Kinch, X. Liu, J. Hu, H. Liu, S. Dai, Mechanochemical-assisted synthesis of high-entropy metal nitride via a soft urea strategy, Adv. Mater. 30 (2018) 1707512, https://doi.org/10.1002/adma.201707512.

[10] T.K. Chen, T.T. Shun, J.W. Yeh, M.S. Wong, Nanostructured nitride films of multi-element high-entropy alloys by reactive DC sputtering, Surf. Coat. Technol. 188–189 (2004) 193–200, https://doi.org/10.1016/j.surfcoat.2004.08.023.

[11] R.-Z. Zhang, F. Gucci, H. Zhu, K. Chen, M.J. Reece, Data-driven design of eco-friendly thermoelectric high-entropy sulfides, Inorg. Chem. 57 (2018) 13027–13033, https://doi.org/10.1021/acs.inorgchem.8b02379.

[12] J. Gild, J. Braun, K. Kaufmann, E. Marin, T. Harrington, P. Hopkins, K. Vecchio, J. Luo, A high-entropy silicide: (Mo0.2Nb0.2Ta0.2Ti0.2W0.2)Si2, J. Materiomics. (2019), https://doi.org/10.1016/j.jmat.2019.03.002.

[13] Y. Qin, J.-X. Liu, F. Li, X. Wei, H. Wu, G.-J. Zhang, A high entropy silicide by reactive spark plasma sintering, J. Adv. Ceram. 8 (2019) 148–152, https://doi.org/10.1007/s40145-019-0319-3.

[14] J. Gild, M. Samiee, J.L. Braun, T. Harrington, H. Vega, P.E. Hopkins, K. Vecchio, J. Luo, High-entropy fluorite oxides, J. Eur. Ceram. Soc. 38 (2018) 3578–3584, https://doi.org/10.1016/j.jeurceramsoc.2018.04.010.

[15] R. Djenadic, A. Sarkar, O. Clemens, C. Loho, M. Botros, V.S.K. Chakravadhanula, C. Kübel, S.S. Bhattacharya, A.S. Gandhi, H. Hahn, Multicomponent equiatomic rare earth oxides, Mater. Res. Lett. 5 (2017) 102–109, https://doi.org/10.1080/21663831.2016.1220433.

[16] J. Dąbrowa, M. Stygar, A. Mikuła, A. Knapik, K. Mroczka, W. Tejchman, M. Danielewski, M. Martin, Synthesis and microstructure of the (Co,Cr,Fe,Mn,Ni)3O4 high entropy oxide characterized by spinel structure, Mater. Lett. 216 (2018) 32–36, https://doi.org/10.1016/j.matlet.2017.12.148.

[17] S. Jiang, T. Hu, J. Gild, N. Zhou, J. Nie, M. Qin, T. Harrington, K. Vecchio, J. Luo, A new class of high-entropy perovskite oxides, Scr. Mater. 142 (2017) 116–120, https://doi.org/10.1016/j.scriptamat.2017.08.040.

[18] C.M. Rost, E. Sachet, T. Borman, A. Moballegh, E.C. Dickey, D. Hou, J.L. Jones, S. Curtarolo, J.-P. Maria, Entropy-stabilized oxides, Nat. Commun. 6 (2015) 8485, https://doi.org/10.1038/ncomms9485.

[19] D.A. Vinnik, E.A. Trofimov, V.E. Zhivulin, O.V. Zaitseva, S.A. Gudkova, A.Yu Starikov, D.A. Zherebtsov, A.A. Kirsanova, M. Häßner, R. Niewa, High-entropy oxide phases with magnetoplumbite structure, Ceram. Int. (2019), https://doi.org/10.1016/j.ceramint.2019.03.221.

[20] X. Ren, Z. Tian, J. Zhang, J. Wang, Equiatomic quaternary (Y1/4Ho1/4Er1/4Yb1/4)2SiO5 silicate: a perspective multifunctional thermal and environmental barrier coating material, Scr. Mater. 168 (2019) 47–50, https://doi.org/10.1016/j.scriptamat.2019.04.018.

[21] G. Tallarita, R. Licheri, S. Garroni, R. Orrù, G. Cao, Novel processing route for the fabrication of bulk high-entropy metal diborides, Scr. Mater. 158 (2019) 100–104, https://doi.org/10.1016/j.scriptamat.2018.08.039.

[22] J. Gild, K. Kaufmann, K. Vecchio, J. Luo, Reactive flash spark plasma sintering of high-entropy ultrahigh temperature ceramics, Scr. Mater. 170 (2019) 106–110, https://doi.org/10.1016/j.scriptamat.2019.05.039.

[23] W.-M. Guo, D.-W. Tan, L.-Y. Zeng, Hao-Li, H.-T. Lin, C.-Y. Wang, Synthesis of fine ZrB2 powders by solid solution of TaB2 and their densification and mechanical properties, Ceram. Int. 44 (2018) 4473–4477, https://doi.org/10.1016/j.ceramint.2017.11.155.

[24] D.-W. Ni, G.-J. Zhang, Y.-M. Kan, P.-L. Wang, Synthesis of monodispersed fine hafnium diboride powders using carbo/borothermal reduction of hafnium dioxide, J. Am. Ceram. Soc. 91 (2008) 2709–2712, https://doi.org/10.1111/j.1551-2916.2008.02466.x.

[25] V. Moradi, L. Nikzad, I. Mobasherpour, M. Razavi, Low temperature synthesis of Titanium diboride by carbothermal method, Ceram. Int. (2018), https://doi.org/10.1016/j.ceramint.2018.07.177.

[26] J. Gu, Z. Ji, S. Shi-Kuan, W. Hao, Y. Shu-Yang, W. Weimin, Z. Jinyong, F. Zhengyi, Dense and pure high-entropy metal diboride ceramics sintered from self-synthesized powders via boro/carbothermal reduction approach, Sci. China Mater. (2019), https://doi.org/10.1007/s40843-019-9469-4.

[27] G.S. An, J.S. Han, J.U. Hur, S.-C. Choi, Synthesis of sub-micro sized high purity zirconium diboride powder through carbothermal and borothermal reduction method, Ceram. Int. 43 (2017) 5896–5900, https://doi.org/10.1016/j.ceramint.2017.01.068.

[28] Y. Zhang, W.-M. Guo, Z.-B. Jiang, Q.-Q. Zhu, S.-K. Sun, Y. You, K. Plucknett, H.-T. Lin, Dense high-entropy boride ceramics with ultra-high hardness, Scr. Mater. 164 (2019) 135–139, https://doi.org/10.1016/j.scriptamat.2019.01.021.

[29] X.-Q. Shen, J.-X. Liu, F. Li, G.-J. Zhang, Preparation and characterization of diboride-based high entropy (Ti0.2Zr0.2Hf0.2Nb0.2Ta0.2)B2–SiC particulate composites, Ceram. Int. (2019), https://doi.org/10.1016/j.ceramint.2019.08.178.

[30] D. Liu, H. Liu, S. Ning, B. Ye, Y. Chu, Synthesis of high-purity high-entropy metal diboride powders by boro/carbothermal reduction, J. Am. Ceram. Soc. 102 (2019) 7071–7076, https://doi.org/10.1111/jace.16746.

[31] D. Liu, T. Wen, B. Ye, Y. Chu, Synthesis of superfine high-entropy metal diboride powders, Scr. Mater. 167 (2019) 110–114, https://doi.org/10.1016/j.scriptamat.2019.03.038.

[32] Y. Zhou, H. Xiang, Z. Feng, Z. Li, General trends in electronic structure, stability, chemical bonding and mechanical properties of ultrahigh temperature ceramics TMB2 (TM = transition metal), J. Mater. Sci. Technol. 31 (2015) 285–294, https://doi.org/10.1016/j.jmst.2014.09.014.

[33] J.L. Braun, C.M. Rost, M. Lim, A. Giri, D.H. Olson, G.N. Kotsonis, G. Stan, D.W. Brenner, J.-P. Maria, P.E. Hopkins, Charge-induced disorder controls the thermal conductivity of entropy-stabilized oxides, Adv. Mater. 30 (2018) 1805004, https://doi.org/10.1002/adma.201805004.

[34] M. Lim, Zs Rak, J.L. Braun, C.M. Rost, G.N. Kotsonis, P.E. Hopkins, J.-P. Maria, D.W. Brenner, Influence of mass and charge disorder on the phonon thermal conductivity of entropy stabilized oxides determined by molecular dynamics simulations, J. Appl. Phys. 125 (2019) 055105, , https://doi.org/10.1063/1.5080419.

[35] X. Yan, L. Constantin, Y. Lu, J.-F. Silvain, M. Nastasi, B. Cui, Hf0.2Zr0.2Ta0.2Nb0.2Ti0.2)C high-entropy ceramics with low thermal conductivity, J. Am. Ceram. Soc. 101 (2018) 4486–4491, https://doi.org/10.1111/jace.15779.

[36] F. Thévenot, Boron carbide—a comprehensive review, J. Eur. Ceram. Soc. 6 (1990) 205–225, https://doi.org/10.1016/0955-2219(90)90048-K.

[37] V.V. Kurbatkina, E.I. Patsera, E.A. Levashov, A.N. Timofeev, Self-propagating high-temperature synthesis of refractory boride ceramics (Zr,Ta)B2 with superior properties, J. Eur. Ceram. Soc. 38 (2018) 1118–1127, https://doi.org/10.1016/j.jeurceramsoc.2017.12.031.

[38] G.-J. Zhang, W.-M. Guo, D.-W. Ni, Y.-M. Kan, Ultrahigh temperature ceramics (UHTCs) based on ZrB 2 and HfB 2 systems: powder synthesis, densification and mechanical properties, J. Phys. Conf. Ser. 176 (2009) 012041, , https://doi.org/10.1088/1742-6596/176/1/012041.

[39] D. Ghosh, G. Subhash, S. Somiya (Ed.), Chapter 3.3 - Recent Progress in Zr(Hf)B2 Based Ultrahigh Temperature Ceramics, second ed., Handb. Adv. Ceram, Academic Press, Oxford, 2013, pp. 267–299 http://www.sciencedirect.com/science/article/pii/B9780123854698000162 accessed October 30, 2015.

[40] M. Beauvy, Stoichiometric limits of carbon-rich boron carbide phases, J. Less Common Met. 90 (1983) 169–175, https://doi.org/10.1016/0022-5088(83)90067-X.

[41] J.K. Sonber, T.S.R.Ch Murthy, C. Subramanian, S. Kumar, R.K. Fotedar, A.K. Suri, Investigations on synthesis of ZrB2 and development of new composites with HfB2 and TiSi2, Int. J. Refract. Metals Hard Mater. 29 (2011) 21–30, https://doi.org/10.1016/j.ijrmhm.2010.06.007.

[42] P. Jiang, X. Qian, R. Yang, Tutorial: time-domain thermoreflectance (TDTR) for thermal property characterization of bulk and thin film materials, J. Appl. Phys. 124 (2018) 161103, https://doi.org/10.1063/1.5046944.

[43] A.J. Schmidt, PUMP-PROBE thermoreflectance, Ann. Rev. Heat Transf. 16 (2013) 159–181, https://doi.org/10.1615/AnnualRevHeatTransfer.v16.60.

[44] D.G. Cahill, Analysis of heat flow in layered structures for time-domain thermoreflectance, Rev. Sci. Instrum. 75 (2004) 5119–5122, https://doi.org/10.1063/1.1819431.

[45] Y.S. Touloukian, E.H. Buyco, Thermophysical Properties of Matter - the TPRC Data Series. Volume 5. Specific Heat - Nonmetallic Solids, THERMOPHYSICAL AND ELECTRONIC PROPERTIES INFORMATION ANALYSIS CENTER LAFAYETTE IN, 1970, https://apps.dtic.mil/docs/citations/ADA951939 accessed October 1, 2019.

[46] Y. Pan, X. Wang, S. Li, Y. Li, M. Wen, DFT prediction of a novel molybdenum tetraboride superhard material, RSC Adv. 8 (2018) 18008–18015, https://doi.org/10.1039/C8RA02324G.

[47] R. Mohammadi, C.L. Turner, M. Xie, M.T. Yeung, A.T. Lech, S.H. Tolbert, R.B. Kaner, Enhancing the hardness of superhard transition-metal borides: molybdenum-doped tungsten tetraboride, Chem. Mater. 28 (2016) 632–637, https://doi.org/10.1021/acs.chemmater.5b04410.

[48] A.L. Chamberlain, W.G. Fahrenholtz, G.E. Hilmas, D.T. Ellerby, High-strength zirconium diboride-based ceramics, J. Am. Ceram. Soc. 87 (2004) 1170–1172, https://doi.org/10.1111/j.1551-2916.2004.01170.x.

[49] W.G. Fahrenholtz, G.E. Hilmas, I.G. Talmy, J.A. Zaykoski, Refractory diborides of zirconium and hafnium, J. Am. Ceram. Soc. 90 (2007) 1347–1364, https://doi.org/10.1111/j.1551-2916.2007.01583.x.

[50] X. Zhang, G.E. Hilmas, W.G. Fahrenholtz, Synthesis, densification, and mechanical properties of TaB2, Mater. Lett. 62 (2008) 4251–4253, https://doi.org/10.1016/j.matlet.2008.06.052.

[51] B. Basu, G.B. Raju, A.K. Suri, Processing and properties of monolithic TiB2 based materials, Int. Mater. Rev. 51 (2006) 352–374, https://doi.org/10.1179/174328006X102529.

[52] B. Mahesh, K. Sairam, J.K. Sonber, T.S.R.Ch Murthy, G.V.S. Nageswara Rao, T. Srinivasa Rao, J.K. Chakravartty, Sinterability studies of monolithic chromium diboride (CrB2) by spark plasma sintering, Int. J. Refract. Metals Hard Mater. 52 (2015) 66–69, https://doi.org/10.1016/j.ijrmhm.2015.04.035.

[53] E. Wuchina, M. Opeka, S. Causey, K. Buesking, J. Spain, A. Cull, J. Routbort, F. Guitierrez-Mora, Designing for ultrahigh-temperature applications: the mechanical and thermal properties of HfB2, HfCx, HfNx and αHf(N), J. Mater. Sci. 39, 5939-5949 https://doi.org/10.1023/B:JMSC.0000041690.06117.34 n.d..

[54] D.L. McClane, W.G. Fahrenholtz, G.E. Hilmas, Thermal properties of (Zr,TM)B2 solid solutions with TM = Hf, Nb, W, Ti, and Y, J. Am. Ceram. Soc. 97 (2014) 1552–1558, https://doi.org/10.1111/jace.12893.

[55] R.G. Munro, Material properties of titanium diboride | NIST, J. Res. NIST JRES (2000) 105 No. 5 https://www.nist.gov/publications/material-properties-titanium-diboride accessed October 1, 2019.

[56] P.S. Kislyi, S.N. L'vov, V.F. Nemchenko, G.V. Samsonov, Physical properties of the boride phases of chromium, Sov. Powder Metall. Met. Ceram. 1 (1962) 441–443, https://doi.org/10.1007/BF00773921.

[57] B. Ye, T. Wen, M.C. Nguyen, L. Hao, C.-Z. Wang, Y. Chu, First-principles study, fabrication and characterization of (Zr0.25Nb0.25Ti0.25V0.25)C high-entropy ceramics, Acta Mater. 170 (2019) 15–23, https://doi.org/10.1016/j.actamat.2019.03.021.

[58] Y.-P. Wang, G.-Y. Gan, W. Wang, Y. Yang, B.-Y. Tang, Ab initio prediction of mechanical and electronic properties of ultrahigh temperature high-entropy ceramics (Hf0.2Zr0.2Ta0.2M0.2Ti0.2)B2 (M = Nb, Mo, Cr), Phys. Status Solidi B, https://doi.org/10.1002/pssb.201800011 0 (n.d.).